Orbital time scale, intra-platform basin correlation, carbon isotope stratigraphy and sea-level history of the Cenomanian–Turonian Eastern Levant platform, Jordan

JENS E. WENDLER[1,2]*, JENS LEHMANN[1] & JOCHEN KUSS[1]

[1]*Department of Geosciences, Bremen University, P.O. Box 330440, 28334 Bremen, Germany*

[2]*Present address: Smithsonian Institution National Museum of Natural History, 10th & Constitution NW, Washington, DC 20560-0121, USA*

**Corresponding author (e-mail: wendler@uni-bremen.de)*

Abstract: Two Cenomanian–Turonian boundary (CTBE) sections (KB3 and GM3) of the Karak–Silla intra-platform basin of the Eastern Levant carbonate platform, Jordan, are correlated based on high-resolution calcimetry. KB3 contains black shales with over 7 wt% total organic carbon (TOC). GM3 was deposited at shallower water depth and reveals four conspicuous gypsum beds used for sea-level reconstruction. Spectral analysis of carbonate content and TOC reveals forcing, mainly by the 100 ka cycle of Earth's orbit eccentricity.

Whole rock stable carbon isotope data show a conspicuous positive $\delta^{13}C$ excursion representing the Oceanic Anoxic Event 2 (OAE2). The carbon isotope records of KB3 and GM3 correspond well with the cycles in the $\delta^{13}C$ record of the global stratotype (GSSP) at Pueblo (USA). The GSSP orbital timescale, thus, can be applied to the Jordan record. Furthermore, all stable isotope events defined in the English chalk reference record are recognized in Jordan. Our orbital model for the Jordan sequence-stratigraphical framework reveals approximately 1.2 (+0.2) Ma duration of a third-order sequence, proposed to represent one cycle of the long obliquity (1.2 Ma). This long-term period is superimposed on three fourth-order fluctuations of 400 ka length (long eccentricity; fourth-order sea-level fluctuations), each of which comprises four carbonate cycles (100 ka eccentricity; fifth-order sea-level fluctuations). Demise of the Levant platform occurred during the phase of decreasing $\delta^{13}C$ values after OAE2 in the interval between the Cenomanian–Turonian (C–T) boundary and the end of the Early Turonian.

The Levant carbonate platform deposits of central Jordan represent a textbook-like shallow-marine platform setting subdivided into intra-platform basins during Cenomanian–Turonian (C–T) times (Kuss *et al.* 2003). The morphological structuring by these basins induced lithologically highly variable successions, especially during black shale deposition that preferably occurred in deeper sub-basins. A correlation of these different successions is possible by means of high-resolution calcimetry and stable carbon isotope stratigraphy. In this paper we present such a correlation that enables the study of three research aspects: a) linking different palaeoenvironments over the C–T boundary interval; b) refining the sequence-stratigraphic model by constructing an orbital time scale; c) correlating the successions to the global record (exemplified for the well-dated C–T boundary interval) in order to eliminate ambiguities in the local stratigraphy. Furthermore, our data support the global picture and estimates of duration of the C–T boundary interval that includes the global Oceanic Anoxic Event 2 (OAE2).

The duration of OAE2 has been the matter of many studies in recent years resulting in a range of values from 320 to 960 ka (Obradovitch 1993; Sageman *et al.* 2006) partly caused by considering different intervals. An orbital timescale for the Pueblo stratotype section was given by Sageman *et al.* (2006) providing a precise time measure for the period investigated in our study. In addition, a comprehensive study of stable carbon isotope records in Europe was given by Jarvis *et al.* (2006) providing a detailed set of isotope events suitable for global correlation. Recently, an orbital model was also presented for the Wunstorf (Germany) section (Voigt *et al.* 2008). This record correlates well with the present results and can be used to support the new hypothesis put forward in the present paper regarding the orbital trigger of third-order sequences.

Geological setting

The Eastern Levant carbonate platform in Jordan is characterized by 300–400 m thick successions of

From: Homberg, C. & Bachmann, M. (eds) *Evolution of the Levant Margin and Western Arabia Platform since the Mesozoic*. Geological Society, London, Special Publications, **341**, 171–186.
DOI: 10.1144/SP341.8 0305-8719/10/$15.00

nodular limestone, massive limestone and laminated limestone with intercalated clay, marl and gypsum beds that were deposited during the Cenomanian and Turonian. According to Schulze *et al.* (2004), carbonate platform demise occurred during the Late Cenomanian and Early Turonian when the deposition of marl and clay became dominant. The sections GM3 (Ghawr Al Mazar) and KB3 (Kuthrubbah) are outcrop sections, about 30 km apart, in the Wadi system cutting east–west into an extended plateau area east of the Dead Sea (Fig. 1).

Palaeogeographically the NW-deepening Levant carbonate platform extended over the passive margin of the Arabo–Nubian shield during C–T times. The sections studied comprise the Upper Cenomanian Hummar Formation and the Upper Cenomanian to Middle Turonian Shueib Formation, which are part of the Ajlun Group (Powell 1989). They represent deposits of an intra-platform basin (Karak-Silla basin) at *c*. 100 km distance from the palaeocoastline of the Arabian Shield. Schulze *et al.* (2003) report a range of facies representing supratidal to shallow subtidal deposits, based on the analysis of a diverse shallow-water benthic association including calcareous algae, rudists, larger benthic foraminifera, oysters and ostracodes of brackish to hypersaline environments (see Morsi & Wendler 2010). The intra-platform basin was connected to the open marine environment and only temporarily experienced restricted conditions (formation of evaporites) during regressions. GM3 had a marginal position, while KB3 represents deeper parts of the Karak–Silla intra-platform basin.

The described facies indicate prolonged phases of low activity of the platform carbonate factory from the Late Cenomanian to Early Turonian. Despite the general carbonate platform setting, the profiles investigated here show only short periods of normal carbonate production, while most parts of the section consist of marls and clays. So, the material represents a depositional system with relatively high siliciclastic input.

Material and methods

For this paper we focus on the interval section metre 47–83 of section GM3 (Ghawr Al Mazar: 31°15′34″N; 35°35′41″E) representing the OAE2. It is part of a mid-Cenomanian to Lower Turonian section published in separate publications (see Morsi & Wendler 2010). The section develops from green clays and marls into a unit of platy, bituminous limestone beds, followed by brown marly clays, grey marls and limestone at the top. A total of 155 samples were collected from the GM3 section interval 47–83 m at sample spacing of 10–25 cm.

Section KB3 (Kuthrubbah: 31°09′13″N; 35°36′06″E) is 25 m thick and comprises an alternation of black shales and platy, bituminous limestone beds, and shows a massive limestone at the top. An interval of about 2.5 m below this topmost limestone could not be sampled owing to poor outcrop conditions. 117 samples were taken with 10–20 cm sample spacing (section metre 0–16 m) and 30–50 cm (above 16 m).

Bulk samples were crushed with an agate mortar. The measurements of the carbonate content and the total organic carbon (TOC) were performed at the Alfred Wegener Institute Bremerhaven, Germany, using a LECO CS-125 carbon–sulphur determinator. For total carbon a LECO CNS-2000 was used. Stable carbon isotopes were measured on bulk carbonate at the isotope laboratory of Bremen University, Germany, using a Finigan MAT 251 mass spectrometer. The results are reported relative to the V-PDB standard.

Thin sections were prepared from limestone samples for microfacies analysis. Standard smear slides were used for determination of coccolith assemblages.

Results

Biostratigraphy

The integrated biostratigraphic framework of Schulze *et al.* (2003) using nannofossils and ammonites, supported partly by larger benthic foraminifera, forms the stratigraphic basis (Fig. 2). The sections comprise nannoplankton zones CC10 and CC11. For details on index species see Schulze *et al.* (2003). A revision of the nannofossil content of all correlated sections previously studied and new analyses resulted in a repositioning of the zone boundary (Fig. 2) based on earlier appearances of the Turonian index fossil *Quadrum gartneri* already in the section part formerly placed in the Late Cenomanian by Schulze *et al.* (2003), taken parallel to the new GM3 section. The ammonite occurrences in the C–T of Jordan (Schulze *et al.* 2004) provide a more detailed biostratigraphy that can be correlated with ammonite zone schemes of Southern Europe (Hardenbol *et al.* 1998), Israel (Lewy 1989, 1990), and the Middle East in general (Lewy & Raab 1976). In conjunction with the isotope record presented here it enables a good time control. The Hummar Formation (section metre 47–56 m, Fig. 2) contains abundant *Neolobites vibrayeanus*, encountered also in the present material at section metre 47.5 m. Wiese & Schulze (2005) stated that the stratigraphic range of *N. vibrayeanus* in Jordan is not yet clear, but as far as biostratigraphical control is given, the species range correlates approximately with the early Late

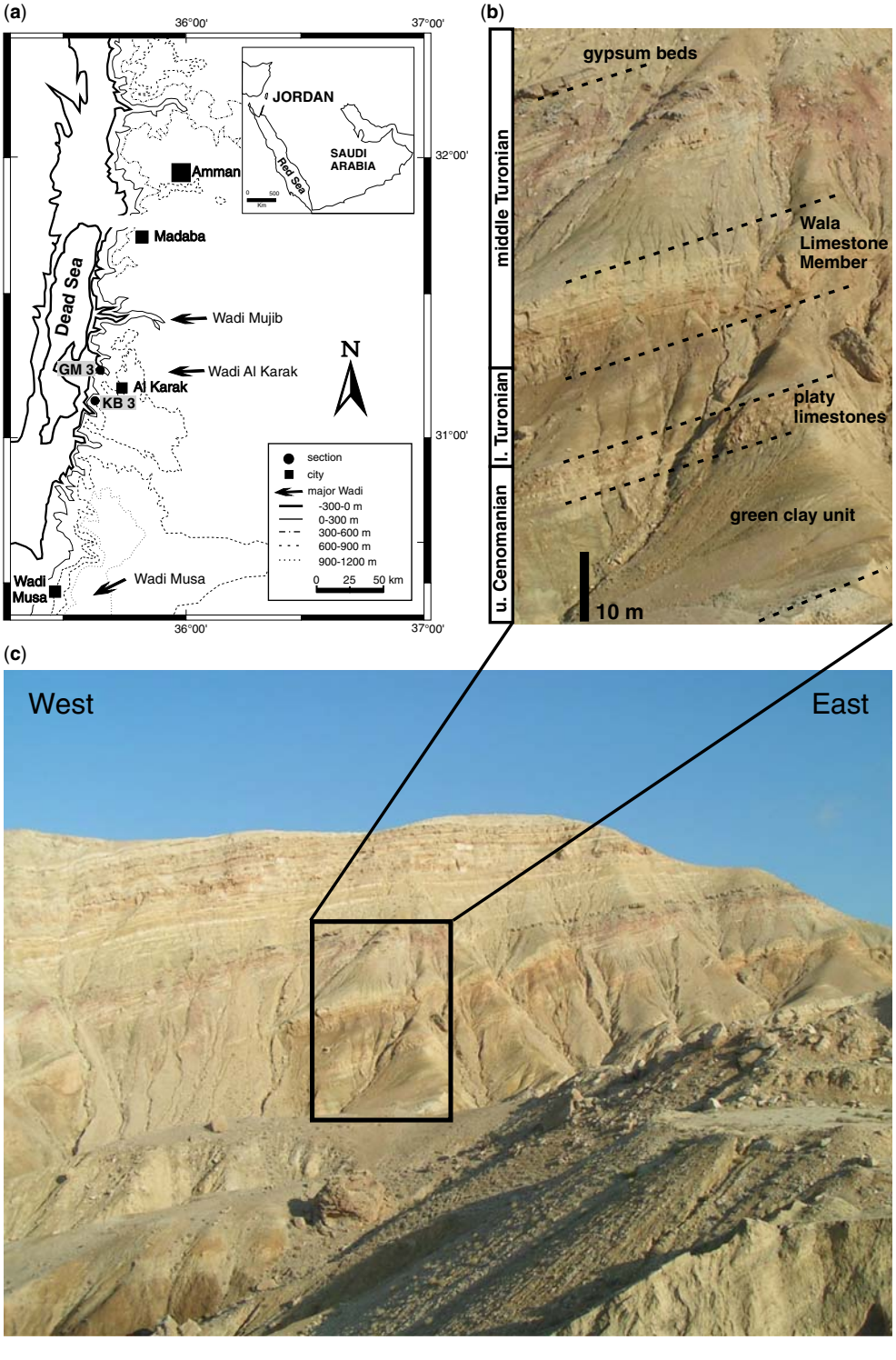

Fig. 1. (**a**) Location of sections GM3 and KB3 in Jordan. (**b**) Investigated section part GM3 showing lithological markers. (**c**) Overview of the northern slope of Wadi Al Karak; frame marks the section enlarged in (b).

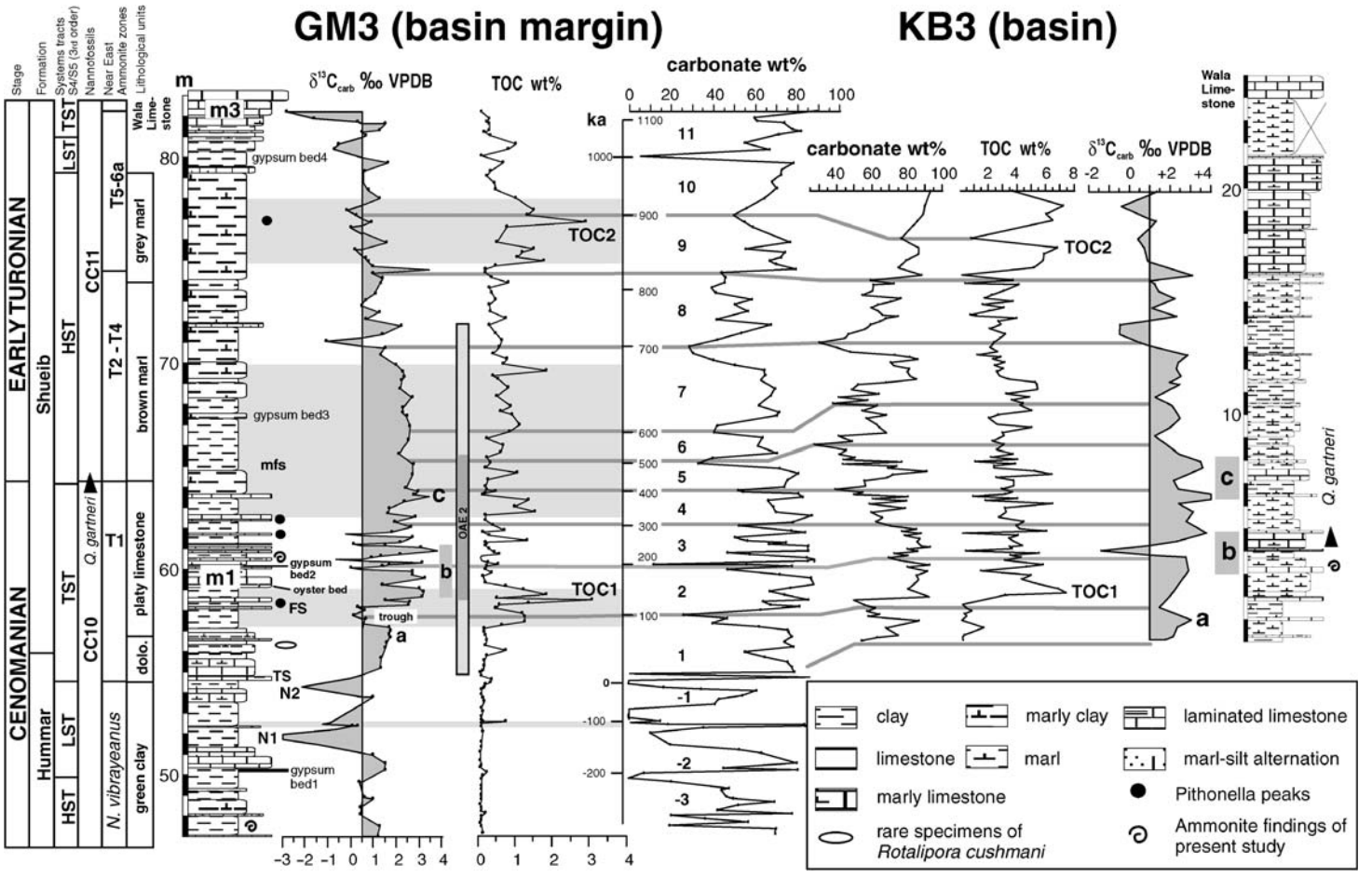

Fig. 2. Biostratigraphy, stable carbon isotope, carbonate and TOC content data of sections GM3 and KB3. Carbonate data connected by correlation lines; lines are extended toward the isotope curves at key points to show correspondence of $\delta^{13}C$ records. TOC, main correlated TOC maxima. Black shales in GM3 = grey shaded intervals. Timescale in the carbonate panel of GM3 assumes 100 ka (eccentricity) duration of the numbered cycles, zero point according to Pueblo (see Fig. 3). Dolo., dolomite unit; TS/FS, transgressive/flooding surface; mfs, maximum flooding surface (according to Schulze *et al.* 2003). Vertical bar marks OAE2 as indicated by Sageman *et al.* (2006). Stratigraphy panel includes the referred lithological units of GM3. m1, m3 – Ammonite marker beds. Positive $\delta^{13}C$ excursions within OAE2: a, b, c; negative $\delta^{13}C$ excursions: N1, N2.

Cenomanian *Calycoceras guerangeri* zone (Lehmann in Wiese & Schulze 2005). Concerning the first occurrence of *N. vibrayeanus*, this is contrary to Schulze *et al.* (2003, fig. 7; 2004, fig. 3) who correlated it in Jordan with the middle of the *Acanthoceras rhotomagense* zone of the northern European zonation. *N. vibrayeanus* is accompanied by further ammonites in Jordan, *Proeucalycoceras haugi*, *Pseudocalycoceras harpax* and *Turrilites acutus*. This assemblage can be assumed to represent Middle to Late Cenomanian (pers. comm. Lewy in Schulze *et al.* 2004). *P. haugi* is a species of the early Late Cenomanian (Kennedy & Juignet 1994). *P. harpax* is also early Late Cenomanian (Kennedy & Juignet 1994), though the delineation between the type material from India and that from the Near East still needs clarification. *T. acutus* mainly occurs in the Middle Cenomanian, and can range into the Late Cenomanian (Juignet & Kennedy 1976). To summarize, the first appearance of *N. vibrayeanus* in Jordan occurs already in the Middle Cenomanian and the last occurrence is correlated with the top of the European *Calycoceras guerangeri* zone.

Section part 56–64 m contains the platy limestone beds described as 'ammonite marker bed 1' by Schulze *et al.* (2003, 2004) who reported *Vascoceras cauvini*, *Metoicoceras geslinianum* and *Burroceras transitorium*, which indicate Near East ammonite zone T1 of Lewy & Raab (1976) correlating with the European *M. geslinianum* and *N. juddii* zones. The record of *B. transitorium* needs further confirmation, since this species is hitherto recorded from New Mexico, Arizona and Brazil only (Kirkland 1996; Gale *et al.* 2005). In the middle part of this interval ammonites are abundant at section metre 60.5 m in section GM3 and at 3.2 m in section KB3. Although most of the specimens are poorly preserved, besides *Puzosia* sp. the largest part can be possibly attributed to very feebly ribbed *Watinoceras* spp., namely *W. guentheri*, *W. hesslandi*, *W. inerme* and *W. semicostatum*. All of these are previously known from western Morocco and western Afrika (Reyment 1955, 1957; Collignon 1967). This group of species might be conspecific following Wright & Kennedy (1981), if so *W. hesslandi* Reyment (1955) has priority. The total range of these smooth *Watinoceras* spp. is poorly known, but the genus is widely accepted as appearing not before the Lower Turonian of the modern substage definition following the discussion of Collignon's (1967) data by (Lehmann & Herbig 2009). The first and possibly most common occurrence of these forms can be placed into the basal Turonian *W. moremani* zone (Wiedmann & Kuhnt 1996), just above the latest Cenomanian *Neocardioceras juddii* zone.

Ammonite zones T2-4 correlate to the basal CC11 and can be only roughly determined by scarce findings of *Choffaticeras pavillieri* and *Ch. quaasi* in section part 67–74 m. The limestone in the top of the section represents the Wala Limestone Member, which was described as 'ammonite marker bed 3' by Schulze *et al.* (2003, 2004). It is characterized at the base by an Early Turonian ammonite assemblage with *Vascoceras durandi*, *Thomasites rollandi*, *Choffaticeras luciae*, *Ch. quaasi* and *Fagesia lenticularis*, indicative of zones T5–6a. The first three species are typical for the *Pseudaspidoceras flexuosum* to *Thomasites rollandi* zones in the middle part of the Lower Turonian in Tunisia, the detailed range of *Ch. quaasi* and *F. lenticularis*, the latter is a somewhat obscure species following Chancellor *et al.* (1994) in the Early Turonian. Transition into zone 6b (*M. nodosoides*/*C. woollgari* zone boundary, base Middle Turonian) was placed by Schulze *et al.* (2003, 2004) in the Middle Wala Limestone.

Lithological evolution at the different intra-platform basin sections

The GM3 section can be subdivided into six lithological units (Fig. 2). Overlying the platform limestone called Karak Limestone, the analysed profile starts at profile metre 47 with a 12 m succession of greenish marls and clays (lower 4.5 m not exposed) with interbedded nodular limestone beds (green clay unit). Occasionally, gypsum beds and crosscutting diagenetic gypsum veins are intercalated at section metre 49–50 m. At 52.30 m a thin (*c.* 15 cm), iron-rich black clay layer marks a first event of increased TOC accumulation (Fig. 2). This bed is very conspicuous in the field and contains a 3 cm thick, very dense, limestone bed. Above this black shale, the succession of greenish clays continues to 54.8 m. A 2.5 m thick unit of dolomite and ankeritized platform carbonate (dolomite unit) follows with a layer of strongly distorted gypsum-carbonate breccia with signs of reworking at the base, possibly connected to a minor hiatus (TS in Fig. 2). It marks an abrupt change in litho- and bio-facies. The section continues into a 7.5 m thick alternation of brownish marl and bituminuous, platy, partly laminated limestone beds (platy limestone unit). The third bed of this unit is an oyster-limestone typical of the platform carbonate facies of the Cenomanian investigated here. The two basal and the upper two bituminuous limestone beds are calcisphere (calcareous dinoflagellate cysts *Pithonella*) packstones showing bioturbation (Fig. 2). The other beds, in contrast, are laminated. Thin sections reveal a strong alteration of the limestone. The dark brown marl at the base of the platy limestone unit forms a second black shale (TOC 1).

This interval is followed by 10 m of monotonous brown clays/marls (brown marl unit). The lower half of this unit can be considered a third black shale. The next unit is a 6 m thick interval of greenish-grey marls (grey marl unit) that contain TOC peak 2 representing the fourth black shale of the section. At section metre 80, a 2 metre thick green to grey, gypsum-rich marl is present. It is followed by a 1 m thick interval of red marls at the base of the following limestone sequence (so-called Wala Limestone). This red marl represents a marine red bed, which potentially is a marker horizon throughout the Levant platform (Wendler *et al.* 2009*a*). The grey, bioclastic Wala Limestone is approximately 14 m thick and represents platform-type carbonate deposits rich in oysters.

Section KB3 is essentially a succession of black shale with intercalated limestones. Section interval 0–5 m displays six equally-spaced, dm-thick, limestone beds, light-beige in colour, alternating with dark-grey marl. Section interval 5–16 m is dominated by dark grey to greenish marl with regular intercalations of dm-thick harder beds. At section metre 16.1 a limestone bed, comparable to the beds in the lower part of the section, is present. From section metre 16.2–24 of the section greenish-grey marl were deposited. The upper part of this unit is barely exposed and strongly weathered and distorted. Thus sampling ends at section metre 20. The Wala Limestone member in the top of the section is dislocated by some metres owing to rock sliding.

Isotope record

Whole rock stable carbon isotopes are in the range of −3 to +4‰ (Fig. 2). High-frequency fluctuations (metre-scale) are evident and a superimposed trend (2–3 m bundles) forms conspicuous negative and positive excursion phases. A broad positive excursion above mean value is present in both sections. The carbon isotope excursion (CIE) of GM3 and KB3 (Fig. 2) shows the following shape (section metres are given for GM3):

- pre-excursion background around 1‰ (with a decreasing trend) in section GM3 part 47–51 m;
- pre-excursion strong negative excursion to −4‰ (section GM3 part 51–54.5 m, double peak: negative peak 1: N1; negative peak 2: N2);
- first build up (peak a) – slow increase to 1.7‰;
- a significant decrease to 0‰ at 57.5 m (the so-called 'trough');
- second build up (peak b) – maximum around 3‰,
- after peak b, a period of significant fluctuation down to 0‰ and below occurs (around 60 m);
- a third build up (peak c) starts around section metre 63 and is part of a plateau of $\delta^{13}C$ values *c*. 2.5‰ from 62 to *c*. 70.5m;
- the post excursion interval 70.5–83 m (slow decrease to mean value), which contains one significant positive excursion of above 3‰ at 74.5 m, and a strong negative excursion to −2.8‰ at 83 m. This negative excursion represents the lowest value since the pre-excursion negative spike.

Calcimetry and gypsum marker beds

In section GM3 carbonate content is between 10 and 90%, and the record shows a distinctive cyclic pattern consisting of high-frequency fluctuations bundled into sets (Fig. 2). These bundles are numbered starting at the base of the isotope excursion. Section part 47–55 m below the isotope excursion can be subdivided into three bundles (−1 to −3) of about 3 m thickness. Abundant disperse gypsum (19%) is present in the clay and marl in the lower and upper parts of bundle −2 (gypsum bed 1). Gypsum content otherwise is generally below 1%. The platy limestone facies (section part 57–64.5 m) shows high-frequency cyclicity in the carbonate content values that range between 50–90%. A conspicuous minimum of 11% carbonate related to elevated gypsum content occurs at bundle boundary 2/3 (gypsum bed 2). From 64.5 m to 80 m the cyclicity continues to show bundling, but bundle thickness increases. At the base of bundle 7 a reddish bed reflects increased contents of iron oxides and gypsum (gypsum bed 3). A bed with a substantial minimum of $<10\%$ carbonate content at 80 m exhibits the highest gypsum content of the section and marks the boundary between bundles 10 and 11 (gypsum bed 4, 69% gypsum). The four so-called gypsum beds are clays and marls with disperse gypsum rather than massive sulphate beds. The most conspicuous one, gypsum bed 4, potentially is connected to a minor hiatus.

TOC is mostly around 0.5 wt% throughout the section (Fig. 2). With the onset of the platy limestone facies related to isotope peak b a 2 m thick peak in TOC (1.5–3%) can be observed (TOC1). Throughout the platy limestone and brown marl units TOC remains around 0.5% with short peaks between 1–2%. Another major peak in TOC straddling about 4 m in thickness (1.5–3% TOC) occurs in the brown marl unit in the carbonate bundles 9 and basal 10 (TOC2).

In the KB3 section carbonate values are between 30 and 95% (Fig. 2). Carbonate content also shows high-frequency cyclicity with superimposed longer-period bundles. The carbonate-minima of these bundles are correlated with the GM3 record. The carbonate cycles of both sections are positively correlated with the cyclic stable carbon isotope excursion.

TOC values abruptly rise from a background level of <1% at the base of the section to a first peak of >7% at 2.5 m (TOC1). Above that level the mean value is constantly decreasing from 4 to 2% and sharply increases to a second major peak of 7% at section metre 18 m to form a 3.5 m thick double peak with maxima of 7% (TOC2). Between these two main peaks TOC values remain high from 5.5 m to 12.5 m with peaks >5%. Similar to the carbonate content, high-frequency cyclicity characterizes the TOC record.

Isotope and calcimetry correlation: spectral analysis

The correlation of carbonate cycles (bundles) between GM3 and KB3 is corroborated by the comparable shape of the $\delta^{13}C$ records and the position of major TOC peaks. Thus, section KB3 comprises cycles 1–10 of GM3. Owing to the high sampling resolution of KB3 the carbonate and TOC records of this section are suitable for spectral analysis in order to determine the type of cyclicity represented.

We estimate mean accumulation rates using possible ages given for the stratigraphic interval studied (based on Ogg *et al.* 2004; Sageman *et al.* 2006) assuming an equal length of the carbon isotope excursion all over the globe. These theoretical accumulation rates are applied to the spectra of carbonate and TOC in order to search for the best fit to the Milankovitch frequency band. According to the Ogg *et al.* (2004) timescale the duration from the base of the Middle Cenomanian to the basal Middle Turonian is about 95.7 to 92.15 = 3.55 Ma. This interval is represented by *c*. 80 m in the GM section (see Schulze *et al.* 2004 for entire section) resulting in 22.5 m/Ma mean accumulation rate. With respect to the isotope excursion the time span between the first increase (peak a) and the end of the plateau is in both time scales about 870–1000 ka (vertical bar in Figs 2, 3 & 4) resulting in mean accumulation rates of 16–19 m/Ma (KB3) and 20–23 m/Ma (GM3). This interval contains eight cycles in both sections. Since cycle thicknesses in GM3 are highly variable (Fig. 2) the range of estimated accumulation rates is larger: cycles 4–6 are ≤2 m thick while all other cycles are 3–3.8 m thick. Thus, accumulation rates around 30 m/Ma dominate.

Power spectra were generated using the Lomb–Scargle algorithm. The TOC spectrum of KB3 (Fig. 5a) shows a strongest power signal at 7.2 m, followed by peaks in power at a 16 m long period (close to section thickness of 20 m: low significance), 2.83 m, 1.65 m, 0.34–0.41 m (only two samples per cycle: low significance). A less significant signal occurs at 0.88 m. Assuming 18 m/Ma mean accumulation rate the 7.2 m cycle would be 400 ka long eccentricity, 2.83 m represents a period of *c*. 200 ka not known from the Milankovitch frequency band. The cycle at 1.65–1.84 m is in the range of short eccentricity, and 0.34–0.41 m would represent precession. The peaks at 0.66 m and 0.88 m could reflect the obliquity cycle.

The spectrum of carbonate content (Fig. 5b) of the most symmetrical, highest resolution part of KB3 (3–11 m) shows two prominent peaks of 1.6–2.65 m cycles. Power is also recorded at a cycle of *c*. 7 m thickness which is, however, about the thickness of the measured section. Two small signals occur at 0.34 m and 0.36 m. Cycle and bed thickness is lower in this part of the sections (Fig. 2). Thus, using 17 m/Ma proposed accumulation rate for this particular interval (derived from high-resolution correlation of Fig. 4) the two strongest peaks are related to 156 and 97 ka, the 7 m cycle spans 400 ka, and the 0.34 m cycle would comprise 20 ka. The cycle ratio 1.6:0.34 m is 4.7:1.

Figure 5c shows the power spectrum of carbonate content of section GM3. Three peaks occur in the frequency band of short eccentricity (2.65 m, 3.3 m, 4.1 m), and strong peaks are present in both the obliquity (1.29 m) and precession (0.71 m and 0.59 m) frequency bands. In Figure 5d the section part 67–79.8 m is analysed. We find the strong 3.42 m cycle (cycles 8–11 in Fig. 2) corresponding to a duration of 107 ka when 32 m/Ma accumulation rate is assumed. This latter analysis suggests that accumulation rates of GM3 are higher than those of KB3, especially in the Lower Turonian part of GM3.

Discussion

High-resolution correlation with Pueblo: an orbital timescale for the Levant

In Figure 3 we attempt a correlation of the Jordan GM3 isotope record with the Pueblo GSSP section record of Sageman *et al.* (2006). We can assume a reasonably complete stratigraphic record based on the lithological properties of the GM3 section, which indicates only two potential positions of minor hiati. Those are, first, the base of the dolomite unit where reworking is indicated, and second, the gypsum bed 4 where a substantial sulphate content suggests enhanced evaporitic conditions during deposition linked to temporary emersion (Wendler *et al.* 2009*a*).

The 100 ka cycles in the carbonate record positively correlate with the $\delta^{13}C$ curve but are more detailed. Thus, we use the clearly defined cycles of the carbonate record and correlate excursions of decreased carbonate content (negative $\delta^{13}C$ excursions) with negative excursions in the Pueblo

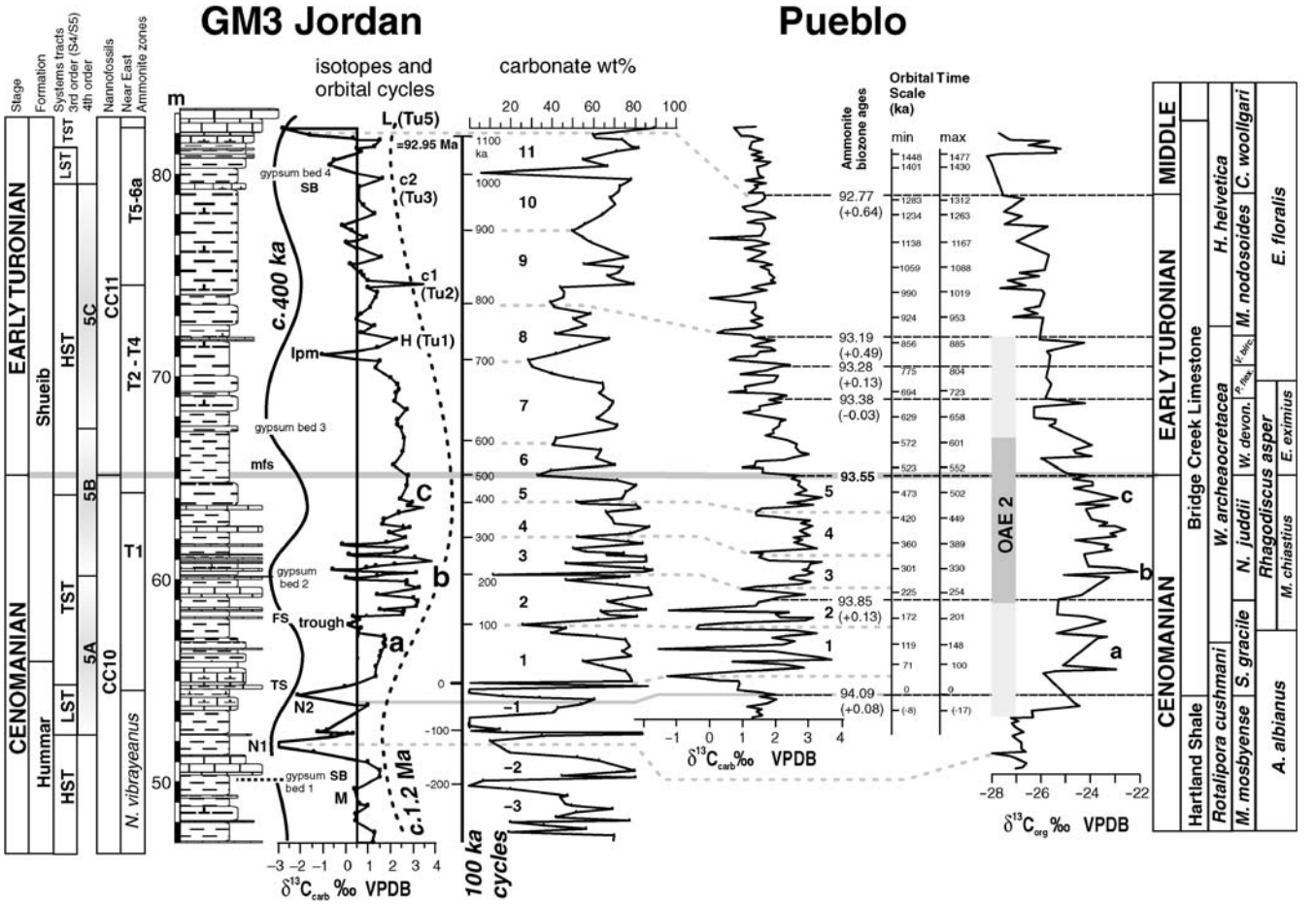

Fig. 3. Correlation of the GM3 section and Pueblo (Colorado) GSSP; Pueblo orbital time scale from Sageman *et al.* (2006); correlation lines use minima in the isotope/carbonate curves. 100 ka-cycle numbering (carbonate curve) indicates Jordan fifth-order cycles; 100 ka-cycle numbers have been suggested accordingly for the Pueblo $\delta^{13}C_{carb}$ record between the base of the CIE and the C–T boundary in concert with the Pueblo orbital model. GM3 isotope record: Isotope events from Jarvis *et al.* (2006) are labelled according to Figure 4: M, Monument; h, Holywell; c1; c2; L, Lulworth; lpm, late plateau minimum (new event introduced here); the respective numbering according to Voigt *et al.* (2006) is TU1 to TU5. Jordan orbital model: stippled curve, 1.2 Ma long-obliquity cycle (third-order sea-level cycle); solid curve, 400 ka long-eccentricity (fourth-order sea-level cycle). In the stratigraphy column, sequence S5 is grey-shaded; 5a, 5b and 5c are the fourth-order sub-sequences according to orbital model; SB = sequence boundary.

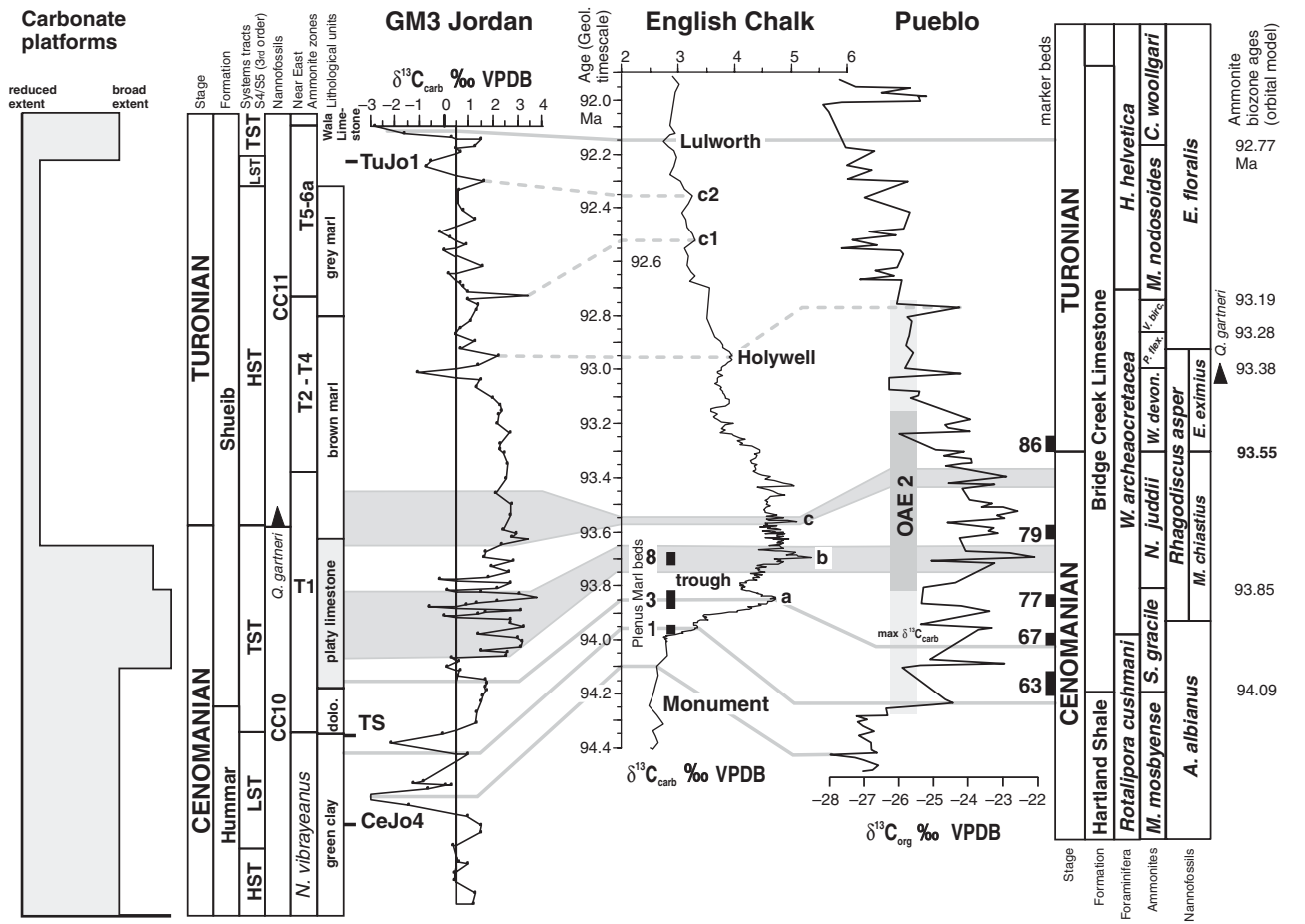

Fig. 4. Correlation of $\delta^{13}C$ records Jordan and Pueblo (Sageman *et al.* 2006) with the English chalk reference curve (Jarvis *et al.* 2006). SB = sequence boundary. Positions of marker beds of Plenus Marl (England) and Bridge Creek Limestone (Pueblo) are given to aid lithological comparison with Jordan (platy limestone unit grey shaded). Left panel: qualitative representation of platform extent redrawn from Philip & Airaud Crumiere (1991).

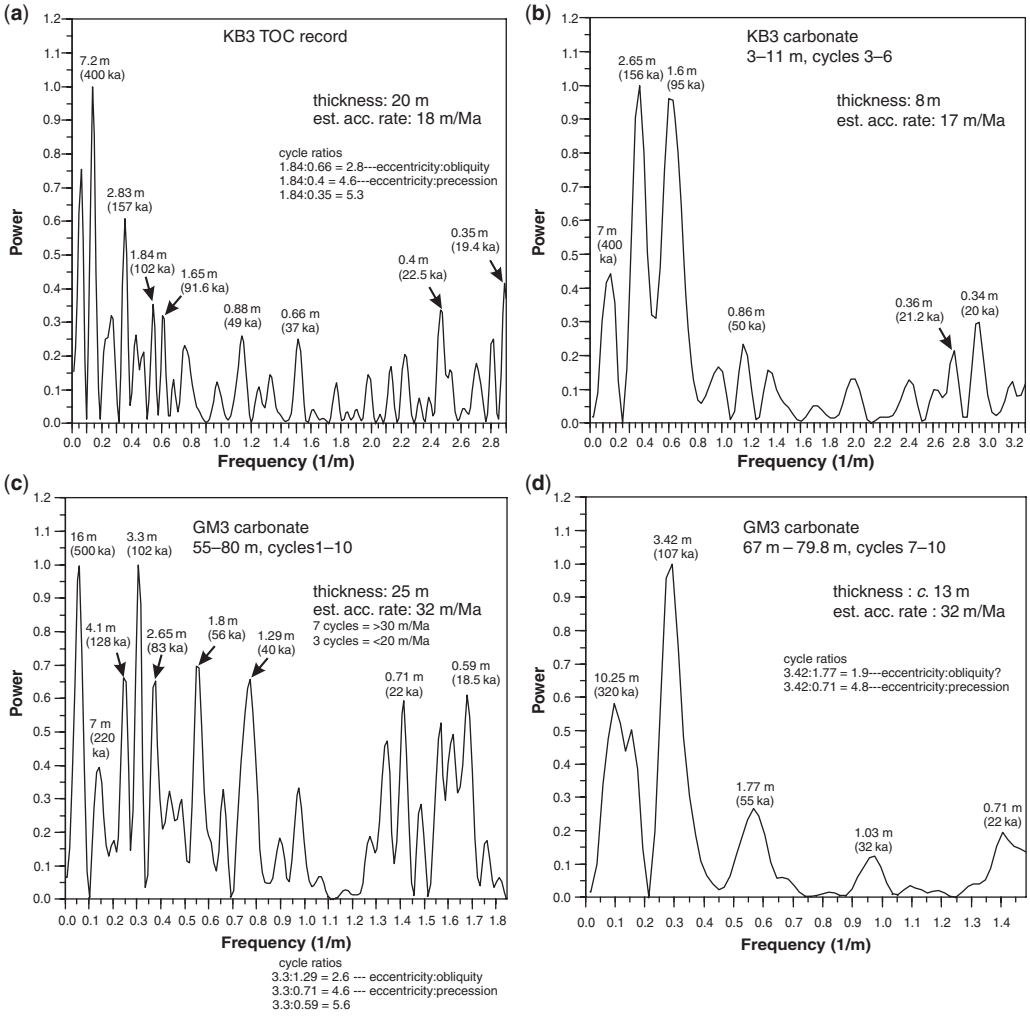

Fig. 5. Power spectra of TOC and carbonate values. (**a**) KB3 TOC record assuming mean accumulation rate of 18 m/Ma. (**b**) KB3 carbonate record of section part 3–11 m (Late Cenomanian). (**c**) GM3 carbonate record. 26 m/Ma mean accumulation rate for this section, dominant cycle thickness >3 m (>30 m/Ma). Match with Milankovitch frequencies occurs at 32 m/Ma accumulation rate. (**d**) Lower Turonian section part of GM3.

$\delta^{13}C$ record (Fig. 3). The spectral analysis strongly supports the idea that, such as in Pueblo, orbital forcing dominated by the 100 ka eccentricity caused the cycles in the Jordan record. Correlation starts at the zero-level of the Sageman *et al.* (2006) orbital time scale, which we interpret to be corresponding to the base of peak a of Jordan based on biostratigraphy and interpretation of the isotope record. Further levels to tie the records are the peak positions b, c in both Jordan and Pueblo.

100 ka cycle lengths of the Pueblo section are determined by the orbital time scale panel in Figure 3. Comparing the number of cycles in the interval from the base of the CIE to the Cenomanian–Turonian boundary (CTB) unfolds a cycle-by-cycle correspondence between the two records. Hence, the five cycles determine a duration of 500 ka for this interval in both records (Fig. 3). This is one cycle longer compared to only four cycles detected by Voigt *et al.* (2008) for the same interval in the Wunstorf (Germany) section. Similarly, slight differences to the Pueblo and Wunstorf records occur in the Early Turonian interval: We have six 100 ka cycles between the CTB and the Lulworth isotope event in Jordan; in Pueblo (800 ka) two more 100 ka cycle were calculated; in Wunstorf a length of 6.25 cycles (100 ka) is seen for that same period of time.

Global carbon isotope events

Figure 4 is based on the correlation in Figure 3 and integrates the English chalk reference record of Jarvis *et al.* (2006) into this correlation in order to identify the isotope events of the latter for the Jordan record. The correlation of peaks a, b and c of the OAE2 between England and Pueblo is followed the one given by Jarvis *et al.* (2006) who used the Pratt (1985) isotope curve for Pueblo. Thus, Figure 4 integrates the detailed stratigraphies of the Plenus Marls (England), Bridge Creek Limestone (Pueblo) and the platy limestone (Jordan), part of which contain the main isotope peaks in the respective regions. The platy limestone unit, together with the dolomite unit below, can be considered the time-equivalent of the Plenus Marl. The facies change, from clays to a conspicuous dolomitic limestone bed, occurs at the base of the isotope excursion. This facies change is interpreted as a transgressive surface (TS) owing to its litho-facies properties and marks the onset of isotope peak a. It can be correlated using stable carbon isotopes with bed 63 of the Pueblo section, and relates to the base of the Plenus Marls. The base of Bed 63 of Pueblo is a TS. Deepening above the mentioned facies change in GM3 is also indicated by bio-facies properties of the platy limestone unit representing a substantial change from a brackish fauna below to an assemblage consisting of normal marine microfaunal elements (compare Morsi & Wendler 2010). Based on the correlation in Figure 4, this onset of a marl–limestone alternation corresponds to Pueblo bed 67 and Plenus Marl bed 3 both covering the 'a' peak of the isotope excursion and indicating progressive onlap.

The continuation of cyclic limestone bed deposition above isotope peak a in Jordan (see also Fig. 3) represents progressive flooding. It is followed by the oyster bed (Fig. 2), which appears to be an equivalent of the 'oyster packstone' of Caus *et al.* (1997), which represents this transgression in the Pyrenees platform of NE Spain. The latter can be related to a major transgressive pulse throughout Europe (e.g. comprehensive overview in Voigt *et al.* 2006). A discrepancy concerning the correlative beds within the CIE peak-interval 'a' occurs in the literature as some studies correlate Plenus Marl bed 3 with bed 63 of Pueblo (Keller *et al.* 2004; Voigt *et al.* 2006), which has implications for the timing of the initial transgression.

The correlation of the Lulworth peak in the top of the three sections is based on the assumption that the *nodosoides*/*woollgari* (resp. T6a/T6b) ammonite zone boundary is synchronous in the three sections as corroborated for Pueblo and England by Kennedy & Cobban (1991) and for the Middle East by Lewy & Raab (1976) and Schulze *et al.* (2003).

Within this correlation scheme a peak by peak correlation is possible for further events. The good fit approached by this procedure (Fig. 4) implies high-resolution correspondence of the three records and the absence of considerable hiatuses in any of them. Besides the positive $\delta^{13}C$ excursions, the double-peaked negative excursion N1 and N2 merits attention. It correlates in timing and shape with a recently described strong negative $\delta^{13}C$ excursion preceding OAE2 in carbonate platform deposits from Mexico (Elrick *et al.* 2009) suggesting a common, perhaps global, cause.

Sea level across the C–T boundary interval: implications of isotope record for sequence stratigraphy

Our sedimentological analysis combined with isotope data implies the following model of sea-level variation (Fig. 3). The four gypsum beds mark periods of evaporitic deposition during times of low sea level. The basal and top one of these gypsum-rich marl beds are the two most conspicuous ones. Thus, we relate them to major third-order lowstands. The lower one relates to sequence boundary CeJo4 of Schulze *et al.* (2004) [corresponding to the global Ce5 of Haq *et al.* (1987) and Haq & Al-Qahtani (2005)]; the upper one near the Early–Mid Turonian boundary is correlated with the globally recognized sequence boundary Tu1 (Fig. 6). CeJo4 marking the base of the fifth Cenomanian sequence (S5) of Jordan was defined by Schulze *et al.* (2004) based on a hardground at the top of the Hummar limestone, which is present in more distal sections while not developed in the study area, where this stratigraphic level is represented by lowstand deposits (green clay unit, Fig. 2) followed by a conspicuous surface marked by the black shale at section metre 52.3 (CeJo4).

Regarding the south-western Levant platform, a sequence boundary corresponding to the global sequence boundary Tu1 in the Early Turonian is present in the Sinai area (CeSin7 of Bauer *et al.* 2003), however, its exact stratigraphic position cannot be determined there owing to a major hiatus. Because of its global significance, this major sequence boundary needs to be newly defined for Jordan. It should be numbered TuJo1 (Fig. 6). Being located near the Early–Mid-Turonian boundary this third-order sequence boundary TuJo1 is, in contrast to Schulze *et al.* (2004), positioned below instead of being above the Wala Limestone Member. This controversy shows the importance of the distinction of fourth-order and third-order sequences in order to

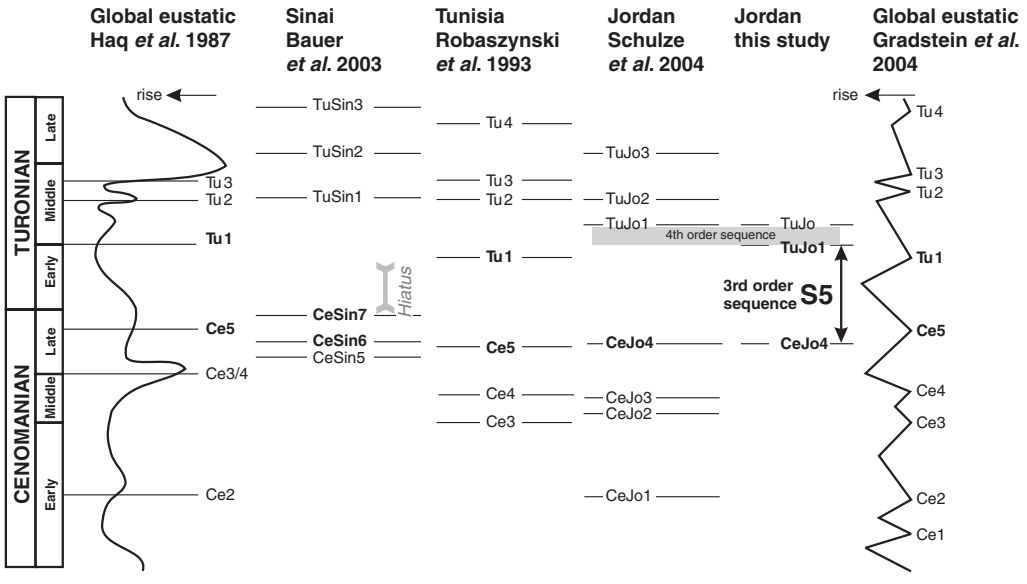

Fig. 6. Overview of sequences at various positions at the Levant platform (Robaszynski *et al.* 1993; Hardenbol & Robaszynski 1998; Bauer *et al.* 2003; Schulze *et al.* 2004) and global sequences (Gradstein *et al.* 2004). Note differences in sequence boundaries of Jordan sequence S5 resulting from distinction of fourth-order and third-order sequences (grey bar).

define co-relatable sequence boundaries. Besides different-scale Milankovitch cycles, as shown in the present case, tectonically controlled local sea-level fluctuations may lead to a mismatch in the inter-plate sequence-stratigraphic correlation approaches (Strasser *et al.* 2000) because they may, independently from the global eustatic control, pronounce sedimentary surfaces. We interpret the sequence boundary in the top of the Wala limestone member, formerly assigned to TuJo1 by Schulze *et al.* (2004), to correspond to a fourth-order sea-level fluctuation and propose the following third-order sequence architecture.

There are four carbonate cycles of 100 ka duration between two gypsum beds (Fig. 3). Hence the sea-level fluctuations between the gypsum rich marl beds follow a 400 ka period that can be assigned to the long eccentricity. This cycle is confirmed by spectral analysis (Fig. 5) although this kind of analysis must be interpreted with care because of the shortness of the analysed section. Consequently, the two major sequence boundaries comprising an interval of 12 carbonate cycles of length 100 ka are 1.2 Ma apart. Hence this is the total duration of third-order sequence S5 of Jordan (Figs 3 & 6). It is composed of three cycles of 400 ka length that are interpreted to represent fourth-order sea-level fluctuations. The 100 ka carbonate cycles apparently were forced by sea-level variations too, as they may show flooding surfaces (FS in Fig. 3) at the base. Therefore, we can interpret short eccentricity to have forced fifth-order sea-level changes.

The carbon isotope record corresponds to this succession of sequences (Fig. 3) – the main negative isotope excursion occurring with a phase difference of about one fifth-order cycle-length (100 ka) after the gypsum beds (i.e. gypsum bed 1 followed by negative spike N1; gypsum bed 4 followed by Lulworth event). Likewise, the two minor minima in the $\delta^{13}C$ record, the interval between $\delta^{13}C$ peaks b and c, and the late plateau minimum (lpm), occur above the fourth-order cycle boundaries, gypsum bed 2 and 3 respectively. Thus, these minima are apparently linked to lowest sea level. Major positive $\delta^{13}C$ excursions correspondingly are positioned between the gypsum beds during transgression and highstand: a and b in sequence 5A; c in sequence 5B; Holywell, c1, c2 in sequence 5C (Fig. 3).

Concluding, based on our cycle analysis and the orbital model for third- to fifth-order sea-level cycles in Jordan we can support the orbital model of Sageman *et al.* (2006). Hence, the Jordan record underpins the notion of Sageman *et al.* (2006) that the Early Turonian comprises about 800 ka, that is, 640 ka less than in the GTS 2004. Regarding the time interval from Monument to Lulworth (approximately corresponding to one third-order sea-level cycle), both the Jordan and

the Pueblo records reveal a duration of 1.2 to *c.* 1.4 Ma, respectively. The recent spectral-analysis-based time scale for the Wunstorf record (Voigt *et al.* 2008) reveals *c.* 12 cycles of 100 ka duration (*c*. 1.2 Ma) for the same period of time.

1.2 Ma long obliquity cycle and third-order sea-level change

There is a long period cycle in Earth's obliquity of *c*. 1.2 Ma length, which has been interpreted to drive glacio-eustatically controlled third-order sequences of the Pliocene–Pleistocene (Lourens & Hilgen 1997), and glacio-eustatic sea-level fluctuations with effects on equatorial bio-productivity in the Oligocene (Wade & Pälike 2004). The 1.2 Ma obliquity cycle was also found to be responsible for Middle Miocene global cooling (Abels *et al.* 2005). Thus, we put forward the hypothesis that the 1.2 Ma obliquity cycle had an influence on third-order sea-level variations in the Cretaceous as well. Cycles of similar duration also occur in the Early–Middle Turonian of the Alps (Wendler *et al.* 2009*b*) stratigraphically continuing the pattern presented here. Wilmsen (2003) considers fourth-order sea-level cycles to be 400 ka eccentricity forced, which consequently relates the third-order sequences to a longer-term cyclicity. This is in accordance with our results. A relation between the main carbon isotope excursions in the English Chalk and eustatic sea-level fluctuations has been demonstrated by Jarvis *et al.* (2002, 2006). A critical point, which is frequently mentioned in this context, is the assumption that these sea-level changes require some ice-volume control, which for the Cretaceous is still contentious (e.g. Miller *et al.* 2005).

The timing and possible cause of platform demise of the Levant carbonate platform

It has been stated that OAE2 was coeval with the widespread demise of carbonate platforms in the Tethyan Realm (Masse & Philip 1981; Schulze *et al.* 2004; Voigt *et al.* 2006). Carbonate platform demise associated with OAE's has also been recorded for other stratigraphic levels, such as the Early Cretaceous (e.g. Föllmi *et al.* 1994; Weissert *et al.* 1998). Our study shows that demise of the platform follows the onset of OAE2 with a considerable time lag. While on the one hand, reduced activity in carbonate production of the Levante carbonate platform in the Jordan research area (Schulze *et al.* 2004) started already in mid-Cenomanian times, we note that on the other hand, platform carbonate production resumes to some extend exactly during OAE2. So in the case of the green clay unit, platform retreat can be related to sea-level drop and the establishment of brackish environments well before OAE2. The demise of carbonate production here was likely caused by the enhanced delivery of terrigenous siliciclastic material spanning an episode of several 100 ka, which probably was a precursor to trigger OAE2. Then, at the base of the isotope excursion (globally correlated with the base of the *M. geslinianium* ammonite zone), that is, with the onset of OAE2, we can observe a short-term re-establishment of platform carbonate production (oyster bed, Fig. 2). This level of platform growth, spanning the maximum phase of OAE 2 (CIE peaks a, b) is very noteworthy because it correlates to the conspicuous coral limestones of the Naqb Limestone Member (Powell 1989), which are found in proximal sections of the Arabian block in Jordan along the palaeocoast of the Levant platform. Furthermore, it is coeval with the Late Cenomanian platform extension event of Philip & Airaud Crumiere (1991), which lasted throughout the Late Cenomanian (Fig. 4). So the problem that arises here is that the major peaks in Jordan CIE are in fact correlated with a re-establishment of carbonate platform-type deposits in conjunction with sea-level rise rather than platform demise. Towards the top of this phase, the start of the global calcisphere bioevent of Hart (1991) marks a change in the environmental conditions (note dots in Fig. 2). From this point, that is, above the C–T boundary, platform demise characterized by the absence of platform carbonates follows, that is, with a time discrepancy of about 500 ka after the onset of OAE2. During this phase, spanning the whole Early Turonian, increased cycle thickness was caused by elevated accumulation rates that might indicate higher accommodation space. This can be assumed to correspond to platform drowning. This phase is characterized by *Pithonella* abundance peaks (Fig. 2) continuing the calcisphere bioevent, and suggesting high productivity (Caus *et al.* 1997; Wendler *et al.* 2002*a*, *b*; Wendler & Willems 2002; Wilmsen 2003). Since the demise of the platform postdates OAE2, it cannot have played any role in triggering the disturbance in the carbon cycle related to the anoxic event and vice versa – a strong time lag is clearly involved.

It is interesting that high bio-productivity apparently is a widespread feature of this phase of carbonate platform retreat (e.g. Hallock & Schlager 1986; Brasier 1995), and in the sections studied here it is particularly well represented by an exceptionally high abundance of chlorophyll-derived pristane and phytane (up to 2 mg g-1 TOC) (Sepúlveda *et al.* 2009). It might reflect a response of the biosphere following fertilization during OAE2. Excess phytoplankton production, however, will have diminished the light transmission of surface

waters, possibly strongly enough for hampering activity of the benthic platform carbonate producers (rudists, corals, larger benthic foraminifera), hence the platform demise. While on the one hand this reduction of the platform growth induced hiatuses in the platform sedimentary record near the C–T boundary elsewhere, for example, Bauer *et al.* (2002), the sedimentary record of the intra-platform basin studied here on the other hand provides a continuous record. Platform growth resumes with the onset of deposition of the Wala Limestone (at the top of the section) comprising the uppermost Lower Turonian and basal Middle Turonian.

Conclusions

The two sections of the Karak–Silla intra-platform basin in Jordan, GM3 and KB3, are conspicuously cyclic as revealed from carbonate, TOC and isotope data, and supported by a symmetrical lithological architecture with repeated intercalations of gypsum beds as indicators of sea-level decrease.

Stable carbon isotope, carbonate and TOC records of these two sections show good correspondence at high-resolution. Carbon isotope curves exhibit a broad positive excursion related to OAE2 and comparable to the global record.

Correlation with the Pueblo GSSP section (Sageman *et al.* 2006) enables the establishment of an orbital timescale for the Jordan sections. Isotope events of the European records can be detected in the Jordan sections, thus supporting the wide significance of these time markers.

Based on the constructed timescale a model of orbitally-forced sea-level fluctuation is presented: The Jordan third-order sequence S5 had a duration of 1.2 Ma and is composed of three fourth-order sequences (400 ka). Fifth-order fluctuations were controlled by the 100 ka eccentricity cycle. Gypsum beds indicate the lowstands of the fourth-order cycles. Negative isotope excursions are related to these levels.

The Jordan and Pueblo timescales correlate precisely during OAE2 thus giving equal age determination for both regions:

Base peak a to top peak c: *c.* 500 ka.

The Early Turonian part from the C–T boundary to the Lulworth event in Jordan consists of six 100 ka eccentricity cycles. For this interval of the section, increased cycle thickness caused by elevated accumulation rates should indicate higher accommodation space during platform drowning during the Early Turonian.

The section interval of GM3 representing the lower part of OAE2 contains indications of platform limestone formation. Thus, demise of the Levant platform only occurred later, namely during the phase of decreasing $\delta^{13}C$ values after OAE2 spanning the Early Turonian. Biological factors (strong phytoplankton productivity) apparently played a dominant role for the ceasing of platform carbonate producers.

A. Masri and the Jordan Geological Survey (NRA) are thanked for providing ideal field campaign logistics. Laboratory facilities at the AWI, Bremerhaven, were made available by R. Stein. This research benefitted from review of an earlier manuscript version by S. Voigt. We thank M. Wilmsen and K. Föllmi for their insightful and constructive reviews. Funding was provided by the Deutsche Forschungsgemeinschaft (grant KU 642/B20-1).

References

Abels, H. A., Hilgen, F. J., Krijgsman, W., Kruk, R. W., Raffi, I., Turco, E. & Zachariasse, W. J. 2005. Long-period orbital control on middle Miocene global cooling: integrated stratigraphy and astronomical tuning of the Blue Clay Formation on Malta. *Paleoceanography*, **20**, 1–17.

Bauer, J., Kuss, J. & Steuber, T. 2002. Platform environments, microfacies and systems tracts of the Cenomanian-lower Santonian of Sinai, Egypt. *Facies*, **47**, 1–26.

Bauer, J., Kuss, J. & Steuber, T. 2003. Sequence architecture and carbonate platform configuration (Late Cenomanian–Santonian), Sinai, Egypt. *Sedimentology*, **50**(3), 387–414.

Brasier, M. D. 1995. Fossil indicators of nutrient levels. 1: Eutroplication and climate change. *In*: Bosence, D. W. J. & Allison, P. A. (eds) *Marine Palaeoenvironmental Analysis from Fossils*. Geological Society, London, Special Publications, **83**, 113–132.

Caus, E., Teixell, A. & Bernaus, M. 1997. Depositional model of a Cenomanian–Turonian extensional basin (Sopeira Basin, NE Spain); interplay between tectonics, eustasy and biological productivity. *Palaeogeography, Palaeoclimatology, Palaeoecology*, **129**, 23–36.

Chancellor, G. R., Kennedy, W. J. & Hancock, J. M. 1994. Turonian ammonite faunas from central Tunisia. *Special Papers in Palaeontology*, London, **50**, 118.

Collignon, M. 1967. Les Cephalopodes cretacés du bassin côtier de Tarfaya. Relations stratigraphiques et paléontologiques. *In*: Collignon, M., Lehman, R., Hottinger, L., Davadie-Crosnier, C. & Oertli, H. J. (eds) *Notes et Mémoires du Service Géologique Maroc*, Rabat, **175**, 7–149.

Elrick, M., Molina-Garza, R., Duncan, R. & Snow, L. 2009. C-isotope stratigraphy and paleoenvironmental changes across OAE2 (mid-Cretaceous) from shallow-water platform carbonates of southern Mexico. *Earth and Planetary Science Letters*, **277**, 295–306.

Föllmi, K. B., Weissert, H., Bisping, M. & Funk, H. 1994. Phosphogenesis, carbon isotope stratigraphy, and carbonate platform evolution along the Lower Cretaceous northern Tethyan margin. *Geological Society of America Bulletin*, **106**, 729–746.

GALE, A. S., BENGTSON, P. & KENNEDY, W. J. 2005. Ammonites at the Cenomanian–Turonian boundary in the Sergipe Basin, Brazil. *Bulletin of the Geological Society of Denmark*, **52**, 167–191.

GRADSTEIN, F. M., OGG, J. G. & SMITH, A. 2004. *A Geologic Timescale*. Cambridge University Press, Cambridge.

HALLOCK, P. & SCHLAGER, W. 1986. Nutrient excess and the demise of coral reefs and carbonate systems. *Palaios*, **1**, 389–398.

HAQ, B. U. & AL-QAHTANI, A. M. 2005. Phanerozoic cycles of sea-level change on the Arabian Platform. *Geo Arabia*, **10**, 127–160.

HAQ, B. U., HARDENBOL, J. & VAIL, P. R. 1987. Chronology of fluctuating sea levels since the Triassic. *Science*, **235**, 1156–1167.

HARDENBOL, J. & ROBASZYNSKI, F. 1998. Introduction to the upper Cretaceous. *In*: DE GRACIANSKY, P. C., HARDENBOL, J., JACQUIN, T. & VAIL, P. R. (eds) *Mesozoic and Cenozoic Sequence Stratigraphy of European Basins.* SEPM Special Publication, **60**, 329–332.

HARDENBOL, J., THIERRY, J., FARLAY, M. B., JACQUIN, T., DE GRACIANSKY, P.-C. D. & VAIL, P. R. 1998. Mesozoic and Cenozoic sequence chronostratigraphic framework of European basins, Cretaceous biochronostratigraphy. *In*: DE GRACIANSKY, P. C., HARDENBOL, J., JACQUIN, T. & VAIL, P. R. (eds) *Mesozoic and Cenozoic Sequence Stratigraphy of European Basins.* SEPM Special Publications, **60**, 3–13.

HART, M. B. 1991. The late Cenomanian calcisphere global bioevent. *In*: GRAINGER, P. (ed.) *Proceedings of the Annual Conference of the Ussher Society. Proceedings of the Ussher Society* **7**; **4**. Ussher Society, Bristol, 413–417.

JARVIS, I., MABROUK, A., MOODY, R. T. J. & DE CABRERA, S. 2002. Late Cretaceous (Campanian) carbon isotope events, sea-level change and correlation of the Tethyan and Boreal realms. *Palaeogeography, Palaeoclimatology, Palaeoecology*, **188**, 215–248.

JARVIS, I., GALE, A., JENKYNS, H. C. & PEARCE, M. A. 2006. Secular variation in Late Cretaceous carbon isotopes: a new $\delta^{13}C$ carbonate reference curve for the Cenomanian–Campanian (99.6–70.6 Ma). *Geological Magazine*, **143**, 561–608.

JUIGNET, P. & KENNEDY, W. J. 1976. Faunes d'Ammonites et biostratigraphie comparée du Cénomanien du nord-ouest de la France (Normandie) et du sud d'Angleterre. *Bulletin de la Société géologique de Normandie*, **63**, 193.

KELLER, G., BERNER, Z., ADATTE, T. & STUEBEN, D. 2004. Cenomanian–Turonian and $\delta^{13}C$, and $\delta^{18}O$, sea level and salinity variations at Pueblo, Colorado. *Palaeogeography, Palaeoclimatology, Palaeoecology*, **211**, 19–43.

KENNEDY, W. J. & COBBAN, W. A. 1991. Stratigraphy and interregional correlation of the Cenomanian–Turonian transition in the Western Interior of the United States near Pueblo, Colorado, a potential boundary stratotype for the base of the Turonian stage. *Newsletters on Stratigraphy*, **24**, 1–33.

KENNEDY, W. J. & JUIGNET, P. 1994. A revision of the ammonite faunas of the type Cenomanian, 6. Acanthoceratinae (*Calycoceras (Proeucalycoceras*), *Eucalycoceras*, *Pseudocalycoceras*, *Neocardioceras*), Euomphaloceratinae, Mammitinae and Vascoceratidae. *Cretaceous Research*, **15**, 469–501.

KIRKLAND, J. I. 1996. Paleontology of the Greenhorn cyclotherm (Cretaceous: Late Cenomanian to Middle Turonian) at Black Mesa, northeastern Arizona. *Bulletin of the New Mexico Museum of Natural History and Science*, **9**, 1–131.

KUSS, H. J., BASSIOUNI, M. A. A., BAUER, J., BACHMANN, M., MARZOUK, A. M., SCHEIBNER, C. & SCHULZE, F. 2003. Cretaceous–Paleogene sequence stratigraphy of the Levant Platform (Egypt, Sinai, Jordan). *In*: GILI, E., NEGRA, M. E. H. & SKELTON, P. W. (eds) *North African Cretaceous Carbonate Platform Systems*. Kluwer Academic Publishers, Dordrecht, Boston, London, 171–187.

LEHMANN, J. & HERBIG, H.-G. 2009. Upper Cretaceous ammonites from the Bou Angueur syncline (Middle Atlas, Morocco) – stratigraphic and palaeobiogeographic importance. *Palaontographica*, **289**, 45–87.

LEWY, Z. 1989. Correlation of lithostratigraphic units in the upper Judea Group (Late Cenomanian–Late Coniacian) in Israel. *Israel Journal of Earth Sciences*, **38**, 37–43.

LEWY, Z. 1990. Transgressions, regressions and relative sea-level changes on the Cretaceous shelf of Israel and adjacent countries. A critical evaluation of Cretaceous global sea-level correlations. *Paleoceanography*, **5**, 619–637.

LEWY, Z. & RAAB, M. 1976. Mid-Cretaceous stratigraphy of the Middle East. *Annales du Musée National d'Histoire Naturelle de Nice*, **4**, 1–19.

LOURENS, L. J. & HILGEN, F. J. 1997. Long-periodic variations in the Earth's obliquity and their relation to third-order eustatic cycles and late Neogene glaciations. *In*: PARTRIDGE, T. C. (ed.) *The Plio-Pleistocene Boundary. Quaternary International*, Pergamon, Oxford, **40**, 43–52.

MASSE, J. P. & PHILIP, P. 1981. Cretaceous coral-rudist buildups of France. *Society of Economic Palaeontologists and Mineralogists*, Special Publications, **30**, 399–426.

MILLER, K. G., WRIGHT, J. D. & BROWNING, J. V. 2005. Visions of ice sheets in a greenhouse world. *In*: DE LA ROCHA, C. L. & PAYTAN, A. (eds) *Ocean Chemistry Over the Phanerozoic and its Links to Geological Processes*. Marine Geology, **217**, 215–231.

MORSI, A.-M. M. & WENDLER, J. E. 2010. Biostratigraphy, palaeoecology and palaeogeography of the Middle Cenomanian–Early Turonian Levant Platform in Central Jordan based on ostracods. *In*: HOMBERG, C. & BACHMANN, M. (eds) *Evolution of the Levant Margin and Western Arabia Platform since the Mesozoic*. Geological Society, London, Special Publications, **341**, 187–210.

OBRADOVITCH, J. 1993. A Cretaceous timescale. *In*: CALDWELL, W. G. E. & KAUFFMAN, E. G. (eds) *Evolution of the Western Interior Basin*. Geological Society of Canada Special Paper, **39**, 379–396.

OGG, J. G., AGTERBERG, F. P. & GRADSTEIN, F. M. 2004. The Cretaceous period. *In*: GRADSTEIN, F. M., OGG, J. G. & SMITH, A. G. (eds) *A Geologic Time Scale*. Cambridge University Press, Cambridge, 344–383.

PHILIP, J. & AIRAUD CRUMIERE, C. 1991. The demise of the rudist-bearing carbonate platforms at the Cenomanian/Turonian boundary; a global control. *In*: MONTAGGIONI, L. F. & MACINTYRE, I. G. (eds) *Reefs as Recorders of Environmental Changes. Coral Reefs* **10; 2**. Springer International, Berlin–Heidelberg–New York, International, 115–125.

POWELL, J. H. 1989. Stratigraphy and sedimentation of the Phanerozoic rocks in Central and South Jordan. Pt.B: Kurnub, Ajlun and Belqa groups. *NRA Geological Bulletin*, **11**, 130.

PRATT, L. M. 1985. Isotopic studies of organic matter and carbonate in rocks of the Greenhorn Marine Cycle. *In*: PRATT, L. M. (ed.) *Fine Grained Deposits and Biofacies of the Cretaceous Western Interior Seaway: Evidence of Cyclic Sedimentary Processes.* SEPM Field Trip Guidebook, Tulsa, **4**, 38–48.

REYMENT, R. A. 1955. The Cretaceous ammonoidea of southern Nigeria and the southern Cameroons. *Bulletin Geological Survey of Nigeria*, **25**, 1–112.

REYMENT, R. A. 1957. Über einige wirbellose Fossilien aus Nigerien und Kamerun, Westafrika. *Palaeontographica*, **109**, 41–70.

ROBASZYNSKI, F., HARDENBOL, J. *ET AL.* 1993. Sequence stratigraphy in a distal environment: the Cenomanian of the Kallat Senan area. *Bull. Centres Recherche Exploration-Production Elf Aquitaine*, **17**, 395–433.

SAGEMAN, B., MEYERS, S. R. & ARTHUR, M. A. 2006. Orbital timescale and new C-isotope record for Cenomanian–Turonian boundary stratotype. *Geology*, **34**, 125–128.

SCHULZE, F., LEWY, Z., KUSS, J. & GHARAIBEH, A. 2003. Cenomanian–Turonian carbonate platform deposits in west central Jordan. *International Journal of Earth Sciences*, **92**, 641–660.

SCHULZE, F., MARZOUK, A. M., BASSIOUNI, M. A. A. & KUSS, J. 2004. The late Albanian–Turonian carbonate platform succession of west-central Jordan: stratigraphy and crises. *Cretaceous Research*, **25**, 709–737.

SEPÚLVEDA, J., WENDLER, J., LEIDER, A., KUSS, J., SUMMONS, R. E. & HINRICHS, K.-U. 2009. Molecular-isotopic evidence of environmental and ecological changes across the Cenomanian–Turonian boundary in the Levant Platform of central Jordan. *Organic Geochemistry*, **40**, 553–568.

STRASSER, A., HILLGÄRTNER, H., HUG, W. & PITTET, B. 2000. Third-order depositional sequences reflecting Milankovitch cyclicity. *Terra Nova*, **12**, 303–311.

VOIGT, S., GALE, A. S. & VOIGT, T. 2006. Sea-level change, carbon cycling and palaeoclimate during the Late Cenomanian of northwest Europe; an integrated palaeoenvironmental analysis. *Cretaceous Research*, **27**, 836–858.

VOIGT, S., ERBACHER, J., MUTTERLOSE, J., WEISS, W., WESTERHOLD, T., WIESE, F., WILLMSEN, M. & WONIK, T. 2008. The Cenomanian–Turonian of the Wunstorf section – (North Germany): global stratigraphic reference section and new orbital time scale for Oceanic Anoxic Event 2. *Newsletters on Stratigraphy*, **43**(1), 65–89.

WADE, B. S. & PÄLIKE, H. 2004. Oligocene climate dynamics. *Paleoceanography*, **19**, 1–16.

WEISSERT, H., LINI, A., FOELLMI, K. B. & KUHN, O. 1998. Correlation of Early Cretaceous carbon isotope stratigraphy and platform drowning events; a possible link? *Palaeogeography, Palaeoclimatology, Palaeoecology*, **137**, 189–203.

WENDLER, J. & WILLEMS, H. 2002. Distribution pattern of calcareous dinoflagellate cysts across the Cretaceous–Tertiary boundary (Fish Clay, Stevns Klint, Denmark); implications for our understanding of species-selective extinction. *In*: KOEBERL, C. & MACLEOD KENNETH, G. (eds) *Catastrophic Events and Mass Extinctions; Impacts and Beyond.* Geological Society of America (GSA), Boulder, CO.

WENDLER, J., GRAEFE, K. U. & WILLEMS, H. 2002*a*. Palaeoecology of calcareous dinoflagellate cysts in the mid-Cenomanian Boreal Realm; implications for the reconstruction of palaeoceanography of the NW European shelf sea. *Cretaceous Research*, **23**, 213–229.

WENDLER, J., GRAEFE, K. U. & WILLEMS, H. 2002*b*. Reconstruction of mid-Cenomanian orbitally forced palaeoenvironmental changes based on calcareous dinoflagellate cysts. *Palaeogeography, Palaeoclimatology, Palaeoecology*, **179**, 19–41.

WENDLER, J., WENDLER, I. & KUSS, H. J. 2009*a*. Early Turonian shallow marine red beds on the Levant carbonate platform (Jordan), Southern Tethys. *SEPM Special Publication*, **91**, 179–187.

WENDLER, I., WENDLER, J., NEUHUBER, S. & WAGREICH, M. 2009*b*. Productivity fluctuations and orbital cyclicity during Early to Middle Turonian development of marine red beds. *SEPM Special Publication*, **91**, 209–221.

WIEDMANN, J. & KUHNT, W. 1996. Biostratigraphy of Cenomanian/Turonian organic carbon-rich sediments in the Tarfaya Atlantic Coastal Basin (Morocco). *In*: *Berichte-Reports Geologisch-Paläontologisches Institut der Universität Kiel (Jost Wiedmann Symposium. Cretaceous Stratigraphy, Paleobiology and Paleobiogeography*, Tübingen, 7–10 March 1996, Abstracts), Kiel, **76**, 195–200.

WIESE, F. & SCHULZE, F. 2005. The upper Cenomanian (Cretaceous) ammonite *Neolobites vibrayeanus* (d'Orbigny, 1841) in the Middle East: taxonomic and palaeoecologic remarks. *Cretaceous Research*, **26**, 930–946.

WILMSEN, M. 2003. Sequence stratigraphy and palaeoceanography of the Cenomanian Stage in northern Germany. *Cretaceous Research*, **24**, 525–568.

WRIGHT, C. W. & KENNEDY, W. J. 1981. The Ammonoidea of the Plenus Marls and the Middle Chalk. *Palaeontographical Society Monographs*, **560**, 134–148.